

# A CONTINUAL DEVELOPMENT METHODOLOGY FOR LARGE-SCALE MULTITASK DYNAMIC ML SYSTEMS

Andrea Gesmundo  
Google Research  
agesmundo@google.com

## ABSTRACT

The traditional Machine Learning (ML) methodology requires to fragment the development and experimental process into disconnected iterations whose feedback is used to guide design or tuning choices. This methodology has multiple efficiency and scalability disadvantages, such as leading to spend significant resources into the creation of multiple trial models that do not contribute to the final solution. The presented work is based on the intuition that defining ML models as modular and extensible artefacts allows to introduce a novel ML development methodology enabling the integration of multiple design and evaluation iterations into the continuous enrichment of a single unbounded intelligent system. We define a novel method for the generation of dynamic multitask ML models as a sequence of extensions and generalizations. We first analyze the capabilities of the proposed method by using the standard ML empirical evaluation methodology. Finally, we propose a novel continuous development methodology that allows to dynamically extend a pre-existing multitask large-scale ML system while analyzing the properties of the proposed method extensions. This results in the generation of an ML model capable of jointly solving 124 image classification tasks achieving state of the art quality with improved size and compute cost.

## 1 INTRODUCTION

The traditional approach to the development of Machine Learning (ML) models assumes a fragmentation of the design and evaluation into multiple disconnected iterations causing inefficient use of available resources and engineering effort. Alternative design choices are normally implemented and tested separately rather than being modularized and integrated in a search space whose exploration can be automated. Furthermore each experimental iteration requires to reset the model’s knowledge to a comparable initial state such as random initialization, thus preventing reuse or accumulation of knowledge across trials. This fragmented development methodology is applied also to aspects such as hyperparameter tuning, as the training is usually repeated multiple times to compare different hyperparameter assignments even for a fixed model design. This approach leads to spend a significant part of the available compute into the training of multiple models that provide no contributions to the final ML solution. Furthermore, it relies on significant human intervention rather than aiming to automate any of the design or tuning exploration.

We propose and demonstrate a methodology that integrates the ML design and the experimental evaluation iterations into the continual expansion of an arbitrary pre-existing ML model. The proposed ML methodology allows any design variation and model knowledge enrichment to be evaluated as an extension of the latest state of the dynamic ML system. Successful extensions can be integrated as base for future experimentation and further extensions. This methodology enables the creation of dynamic multitask systems at a scale that would not be feasible to achieve with the constraint of running parallel repetitions from a neutral start state.

The two major contributions of the presented work are:

- **A novel method for the generation of multitask dynamic systems:** We define a set of design and method extensions applicable to the  $\mu$ 2Net method (Gesmundo & Dean, 2022b), that provide improvement and generalization of different aspects such as: multi-factor model

scoring, evolutionary agent capabilities and automated hyperparameter tuning (Section 3). We refer to the novel method to as  $\mu$ 2Net+. The novel methods capabilities are first analyzed by using the traditional ML methodology on a smaller scale for feasibility (Section 4).

- **A novel ML development methodology integrating design and evaluation into the continual and unbounded extension of an ML system.** We demonstrate empirically the effectiveness of the proposed methodology by incrementally extending the model generated by the experiments described in Gesmundo & Dean (2022b). The model is incrementally enriched as the  $\mu$ 2Net+ improvements are introduced and as additional tasks are learned. This large scale continual experiments allows to analyze the effects of the method improvements (as done with the traditional methodology), while also continually extending the model into a large-scale multitask ML system capable of learning 124 image classification tasks with approximately state of the art quality and improved size and compute efficiency. (Section 5).

## 2 RELATED WORK

Many methods have been proposed to achieve dynamic architecture extensions (Chen et al., 2016; Cai et al., 2018), some also focusing on an unbounded stream of tasks (Yoon et al., 2018), some achieving immunity from catastrophic forgetting (Rusu et al., 2016; Rosenfeld & Tsotsos, 2020) or optimizing for quality/cost trade-offs (Tan et al., 2019) (refer to Appendix A for an extended survey). Though, a methodology that integrates the continuous development of methods for dynamic architecture extensibility and knowledge enrichment of a multitask ML system jointly with the human design and experimentation process has not yet been proposed.

Berner et al. (2019) describes a methodology that allows for the continued variation of model architecture and training method while preserving its knowledge. Although, the dynamic architecture extension capabilities are not provided by the definition of higher level abstractions but rather require *surgery* operations requiring custom human intervention. Berner et al. (2019) tackles a single high-complexity task, and the ability of exploring architecture and method variations without resetting the knowledge is deemed a critical accelerator in such context. Advancements in ML models dynamicity, extensibility and reusability can contribute to accelerate progress toward further high-complexity achievements such as "Artificial General Intelligence" (AGI).

The ability of jointly solve a large amount of tasks is another theme that is commonly associated with progress toward AGI. Advancements in scaling language models (Brown et al., 2020; Thoppilan et al., 2022) allowed to achieve discourse and reasoning capabilities that can be applied to new tasks without requiring additional training. Recent work aims to extend these achievements beyond text modality by defining static architectures for an extended subset of modalities (Alayrac et al., 2022; Reed et al., 2022). These are few examples of the ML models contributing to the line of research achieving incremental milestone toward AGI. Though, each models is trained from scratch with considerable resources consumption. The introduction of abstractions allowing to modularize, dynamically extend and reuse these large models may contribute to accelerate the rate of innovation.

## 3 METHOD

The proposed method extends  $\mu$ 2Net (Gesmundo & Dean, 2022b) with the intent of generalizing and improving its capabilities. In this section we detail the four method extensions introduced with  $\mu$ 2Net+: 1) multi factor scoring function, 2) improved hyperparameters search space, 3) additional mutation actions, 4) learned  $\mu(\cdot)$  function. Refer to Gesmundo & Dean (2022b) for a detailed definition of the  $\mu$ 2Net method being extended.

The first method extension consists of the introduction of a new **multi factor scoring function** that integrates additional size and compute penalty factors by employing an exponential decay penalty:

$$score(m) = q(m) * s^{\left(\frac{\#accounted-params(m)}{P}\right)} * s^{\left(\frac{\#flops(m)}{F}\right)} \quad (1)$$

$q(m)$  denotes the quality metric achieved by model  $m$  on the validation set.  $s \in ]0, 1]$  is the cost penalties scaling factor.  $\#flops(m)$  denotes the amount of floating point operations required by model  $m$  at inference time, and  $\#accounted-params(m)$  is the sum of parameters used by model  $m$ , dividing each parameter count by the number of models sharing its use:

$$\#accounted-params(m) = \sum_{p \in \mathcal{P}(m)} \frac{1}{\#models(p)+1} \quad (2)$$

Table 1: Hyperparameters search space. Sequences of valid values for each automatically tunable hyperparameter. Bold vales are defaults. Underlined values are additional values or changes of defaults in comparison to the search space defined by  $\mu$ 2Net.

---

<i>Optimizer hyperparameters</i>
Learning rate $\in$ [0.0001, 0.0002, 0.0005, 0.001, 0.002, 0.005, <b>0.01</b> , 0.02, 0.05, 0.1, 0.2, 0.5]
Learning rate schedule warm up ratio $\in$ [ <u>0</u> , 0.01, 0.02, 0.05, <b>0.1</b> , 0.2, 0.3]
Momentum $\in$ [0.5, 0.6, 0.7, <u>0.75</u> , 0.8, 0.85, <b>0.9</b> , 0.95, 0.98, 0.99]
Nesterov update $\in$ [ <b>False</b> , True]

---

<i>Data Preprocessing hyperparameters</i>
Cropped area range min $\in$ [ <u>0.05</u> , 0.5, <u>0.95</u> , <b>1.0</b> ]
Cropped aspect ratio range min $\in$ [0.5, 0.75, <u>1.0</u> ]
Flip left/right $\in$ [ <b>False</b> , True]
Brightness delta $\in$ [ <b>0.0</b> , 0.01, 0.02, 0.05, 0.1, 0.2]
Contrast delta $\in$ [ <b>0.0</b> , 0.01, 0.02, 0.05, 0.1, 0.2]
Saturation delta $\in$ [ <b>0.0</b> , 0.01, 0.02, 0.05, 0.1, 0.2]
Hue delta $\in$ [ <b>0.0</b> , 0.01, 0.02, 0.05, 0.1, 0.2]
Image quality delta $\in$ [ <b>0.0</b> , <u>0.01</u> , <u>0.02</u> , <u>0.05</u> , <u>0.1</u> , <u>0.2</u> ]
Image resolution pixels $\in$ [ <u>224</u> , <b>384</b> ]

---

$\mathcal{P}(m)$  denotes the set of all parameters used by  $m$ .  $\#models(p)$  denotes the count of models for tasks different from the task  $m$  is trained on, that are currently sharing the use of parameter  $p$ . Intuitively, if  $s = 0.99$ , then a relative reduction of 1% of the quality metric is applied if a tasks is accounted for  $P$  parameters or requires  $F$  flops.

The base  $\mu$ 2Net method allows for 2 types of **mutation actions**: 1) any layer from the parent model can be cloned to create a trainable copy carrying its parameters and optimizer state (e.g. momentum statistics), any other layer is shared in a frozen state, 2) any hyperparameter value can be changed to one of the neighbouring values in the sequence of valid values defined by the search space (see Table 1).  $\mu$ 2Net+ includes a third mutation type, layer removal: the top transformer layer of the parent model can be removed from the sequence of layers defining the child models (see Figure 1). The addition of this mutation type allows to sample models with a number of transformer layers that is smaller than the number of layers of the root model. This allows to generate models using less parameters and compute, thus introducing an additional degree of freedom to optimize for the introduced cost factors.

The hyperparameters **search space extension** includes different types of additions (see Table 1). All the models generated by  $\mu$ 2Net are constrained to use 384 pixels image resolution. This is the resolution recommended for ViT fine-tuning (Steiner et al., 2021). Although the ViT model we are using as a root model has been pretrained on 224 resolution. We extend the search space to include the option of using 224 resolution. This provides an additional option to generate models requiring less compute, as one of the objectives of the empirical study is to analyze the quality/compute trade-off. The options for image preprocessing are extended by adding the possibility to alter the image quality. This is a commonly used technique that was not included in the recommended fine-tuning setup (Steiner et al., 2021) and therefore was not included in  $\mu$ 2Net search space. Though, we find that this new preprocessing function is learned to be activated for a significant portion of the generated models configuration even if set as inactive by default (see Figure 5). Rarely used values have been removed. Steiner et al. (2021) recommends a mild preprocessing configuration for ViT fine-tuning. The preprocessing hyperparameter default values for  $\mu$ 2Net search space were set to match the recommended configuration. Instead,  $\mu$ 2Net+ set the default values to disable all the preprocessing. This change is based on the observation done during preliminary experiments that preprocessing can moderately benefit most of the tasks, but it can have critical negative impact for a subset of tasks. New values have been added to the valid values ranges of some hyperparameters based on observations done over the distributions learned in previous experiments such as those reported in Gesmundo & Dean (2022b). For example, the most common selected value for the "learning rate schedule warm up ration" was the edge value of 0.01, thus the range has been extended by adding the value 0, that allows to disable the learning rate warm up. Also notice that  $\mu$  has been removed from the search space as a hyperparameter since it is now defined as a learnable function conditioned on the mutation type, as described in the following paragraph.

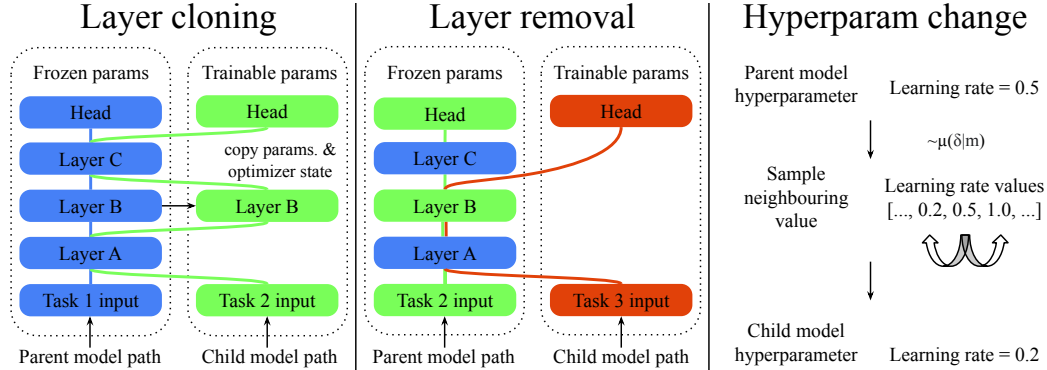


Figure 1: Graphical representation of the three types of mutations defined by the proposed method. New models are generated by applying a sampled subset of possible mutations.

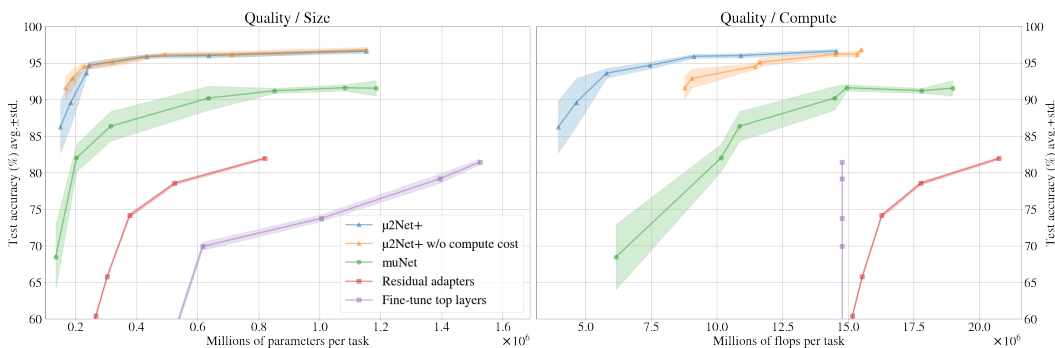
In Gesmundo & Dean (2022a) the mutation sampling is parameterized by a global mutation probability constant  $\mu$ . Gesmundo & Dean (2022b) extends the approach by defining  $\mu$  as a per model hyperparameter tuned by the evolutionary method, thus enabling the selection of distinct mutation probabilities for each model and adapt their value through time.  $\mu$ 2Net+ allows for further per action customization of the learned mutation probabilities by defining a  $\mu$  function,  $\mu(\delta|m)$ , for each model  $m$ . This function maps each mutation action,  $\delta$ , to the probability of applying the mutation action. This extension enables the selection of a distinct mutation probability for each possible mutation action. In practice, the  $\mu$  function is implemented as look-up table mapping every possible mutation to a distinct mutation probability value. The values of the lookup table are inherited and mutated across generations following the same incremental value mutation logic applied to the hyperparameters. All the values in the lookup table are initialized to 0.2, and the sequence of valid mutation probability values is defined as the multiples of 0.02 in the range  $[0.02, 0.3]$ .

#### 4 PARALLEL TRAINING COMPARISON

In this section we use the standard ML methodology to compare different methods by running parallel replicated experiments each using comparable configuration and amount of compute. In particular we focus on quality/cost trade-off comparison. Thus, we compare against common baseline methods that allow to explore the Pareto frontier of such trade-offs. We compare against the muNet method (Gesmundo & Dean, 2022a), and against standard transfer learning techniques such as fine-tuning and residual adapters that provide a cover of the considered trade-off spectrum. As the proposed method introduces the joint optimization of quality, size and compute, we consider two trade-offs: quality/size and quality/compute.

For comparability, the experiment setup and benchmarks are equivalent to those defined in Gesmundo & Dean (2022a) and are summarized in this paragraph. To test the generality of the results, we repeat the experiments on 2 benchmarks: 1) the Multitask Character Classification Benchmark (MCCB), composed by 8 character classification tasks, 2) the Visual Domain Decathlon Benchmark (VDDDB), composed by the 10 tasks of the Visual Domain Decathlon challenge. The VDDDB is more computationally intensive and tasks have been selected to represent a diverse set of domains (see Table 5 for datasets details and references). Experiments are run on TPUv3 with 8 parallel cores. Each experiment is repeated multiple times to measure variance: 5 times for MCCB and 3 times on VDDDB (the lower number of repetitions is due to the higher experiment cost). Every experiment is allocated an equivalent training budget in terms of training epochs per task. Epochs are capped to 51200 training samples for all datasets to smooth the distribution of compute over the set of tasks. For muNet and  $\mu$ 2Net+ models different trade-offs are achieved by setting the scale factor,  $s$ , to different values in the set:  $\{0.02, 0.3, 0.7, 0.9, 0.95, 0.98, 1\}$ . For the Residual adapters baselines, different trade-offs are achieved by changing the inner dimension of each adapter to different values in the set:  $\{8, 16, 32, 64, 128, 256, 512\}$  and all the non residual adapter layers are frozen and shared across models for different tasks. While, for the Fine-tune top layers baseline, different trade-offs

## Multitask Character Classification Benchmark



## Visual Domain Decathlon Benchmark

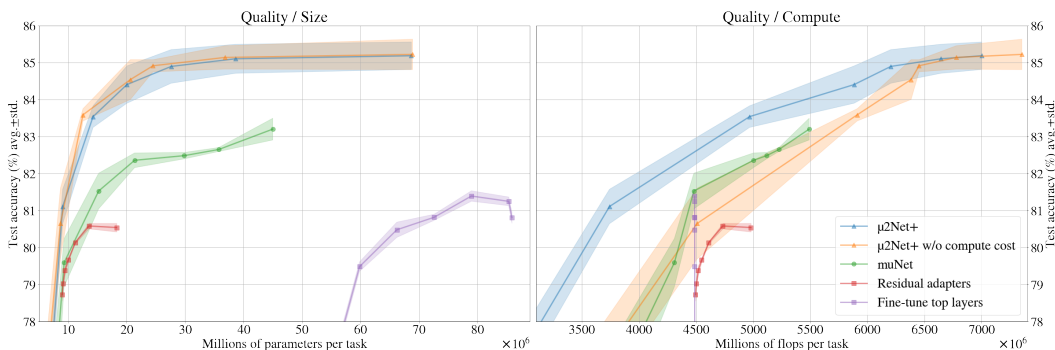


Figure 2: Pareto frontiers achieved in the quality/size and quality/compute spectrum by  $\mu 2\text{Net}+$  and baseline methods on the Multitask Character Classification Benchmark and the Visual Domain Decathlon Benchmark (see Section 4).

are achieved by freezing an increasing number of bottom layers, and again all the frozen layers are shared across multiple tasks to decrease the average number of parameters per task.

The only difference between the experiment configuration of the baseline  $\text{muNet}$  method and the proposed  $\mu 2\text{Net}+$  method is in how the equivalent training budget is distributed. For  $\mu 2\text{Net}+$ , the training budget is distributed to perform more but shorter task iterations. The motivation for this change is to bring the ratio between number of task iterations and length of each iteration closer to what would be representative of the setup for a long term continual learning experiment, that require a significantly higher number of task iterations than the 2 that were originally allocated to  $\text{muNet}$  experiments. Thus we change the distribution to increase the similarity with the setup used by the large scale experiments reported in Gesmundo & Dean (2022b) and their extension with the novel methodology reported in Section 5. These experiments perform 4 training epochs per generation, 4 generations per task iteration and allow for an unbounded number of task iterations. In details, the training budget distribution change consists of: for the MCCB,  $\text{muNet}$  is configured to perform 2 task iterations, 8 generations for each task iteration and each model is trained for 5 epochs, while  $\mu 2\text{Net}+$  performs 5 task iterations, 4 generations for each tasks, and 4 training epochs per model, totalling the same amount of training epochs per task. While, for the VDDB,  $\text{muNet}$  is configured to perform 2 task iterations, 8 generations for each task iteration and each model is trained for 30 epochs, while  $\mu 2\text{Net}+$  performs 30 task iterations, 4 generations for each tasks, and 4 training epochs per model.

The  $\mu 2\text{Net}+$  size cost factor is configured with parameters equivalent to those used for  $\text{muNet}$ :  $P = 1.48\text{M}$  for MCCB and  $P = 85.6\text{M}$  for VDDB proportionally to the number of parameters in the root model. While for the compute cost factor we set:  $P = 15\text{M}$  for MCCB and  $P = 100\text{M}$  for VDDB proportionally to the inference flops required the root model with an image size of the higher end of the allowed range.

The results are represented graphically in Figure 2. The overall comparison shows that the proposed method outperforms all the baseline methods in both benchmarks across both the quality/size and

Table 2: Methods comparison on the MCCB and VDDB task-sets. The metrics of the configuration achieving the best quality are reported for each method. Quality is measured as the test accuracy averaged across tasks. The table reports the max, average and standard deviation of the quality achieved by the experiment repetitions. Model size is measured as the average number of parameters per tasks. Compute is measured as average inference flops.

Model	Test Acc. %		Params/task ( $\times 10^6$ )	Flops/task ( $\times 10^6$ )
	Max	Avg. $\pm$ Std.		
<i>Multitask Character Classification Benchmark</i>				
Full fine-tuning	82.20	81.46 $\pm$ 0.40	1.53	14.77
Residual adapters dim=512	82.28	81.98 $\pm$ 0.17	0.82	20.76
muNet	92.98	91.41 $\pm$ 1.06	1.20	16.64
$\mu$ 2Net+	97.05	96.65 $\pm$ 0.27	1.15	14.55
<i>Visual Domain Decathlon Benchmark</i>				
Fine-tune above 1st tr. layer	81.51	81.39 $\pm$ 0.14	78.98	4485
Residual adapters dim=256	80.67	80.58 $\pm$ 0.07	13.56	4734
muNet	83.58	83.20 $\pm$ 0.29	45.00	5490
$\mu$ 2Net+	85.56	85.19 $\pm$ 0.37	68.70	7001

quality/compute spectrum. We also compare with a version of  $\mu$ 2Net+ without compute cost factor. In the quality/size spectrum we observe that the addition of the compute cost factor does not alter significantly the achieved Pareto frontier. While, we notice a significant gain in the quality/compute trade-off. For example, notice that  $\mu$ 2Net+ without compute cost factor does not outperform muNet in lower end of the quality/compute spectrum for the VDDB experiments. The metrics of the configurations achieving the best quality for each method are reported in Table 2.

It is also interesting to notice that the curves representing the Pareto frontier achieved by Fine-tune top layers becomes a vertical line in the quality/compute spectrum, because the inference compute is independent from the number of layers that are frozen and shared. Also notice that the Residual adapters Pareto frontier outperforms the Fine-tuning one in the quality/size domain. That is expected since Residual adapters are usually employed as a parameter-efficient transfer-learning technique. Although, the order is inverted in the quality/compute spectrum, since Residual adapters add compute cost on top of the root model.

## 5 CONTINUAL MODEL EXTENSION

In this section we describe and demonstrate the proposed continual development methodology that aims to analyze the properties of method and knowledge augmentations through a sequence of experiments while dynamically extending a single large-scale ML model. With this methodology, we aim to characterize and quantify the effects of the introduced extensions by measuring changes thought time, rather than comparing the metrics achieved by parallel runs of method variations (as done with the methodology used in Section 4). The proposed continual development approach has the following advantages:

1. allows to focus all the available compute on the enrichment of a single ML system, thus increasing the accessibility of larger scale experiments,
2. lifts the requirement of training multiple model variations that do not contribute to the final solution for the tasks at hand,
3. enables the unbounded extension of dynamic large-scale multitask systems as the one considered in this section, since it would not be feasible at this scale to train multiple randomly initialized copies of such systems to evaluate each method variation that can be interesting to analyze.

The following experiments also demonstrate how the proposed  $\mu$ 2Net+ method can be applied to extend a pre-trained multitask system generated with a different method. The large-scale multitask system generated by the experiments described in (Gesmundo & Dean, 2022b) is used as the *starting*

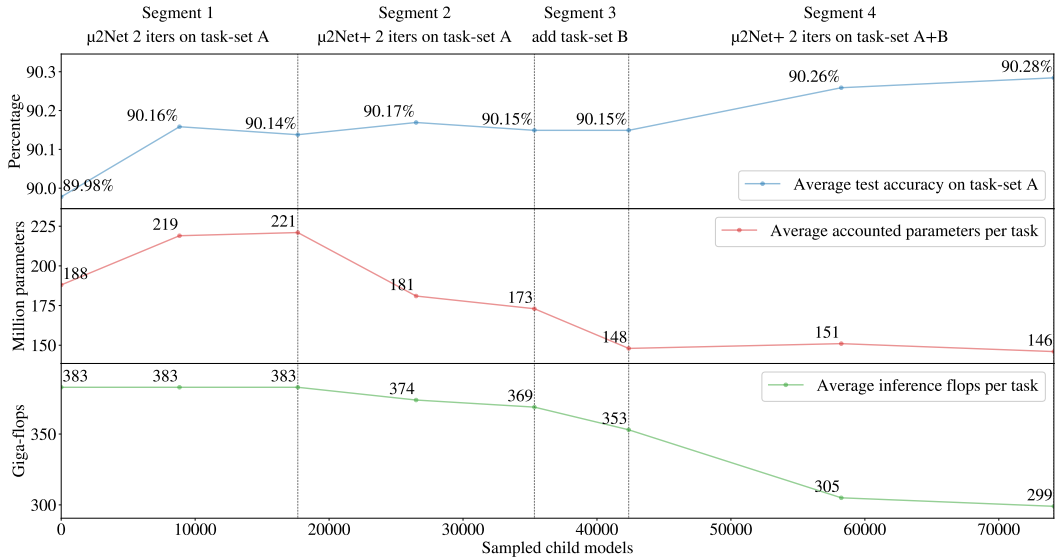


Figure 3: Displays variations through the sequence of experiment segments of 3 reference metrics: 1) Average test accuracy on the task-set A, defined as the initial 69 image classification tasks introduced in Gesmundo & Dean (2022b), notice that the reported test accuracy is computed on a test set that does not overlap with the training set and validation set (whose validation accuracy is used for the reward computation) to avoid overfitting and selection bias. 2) Accounted parameters averaged across all the models composing the multitask system at the time of measure (not limited to task-set A). This measure corresponds to the size cost factor included in  $\mu$ 2Net+ reward function (see Section 3). 3) Compute cost measured as flops required to produce inference for one input sample, also averaged across all the models composing the multitask system at the time of measure (not limited to task-set A). This measure corresponds to the compute cost factor included in  $\mu$ 2Net+ reward function (see Section 3).

*multitask system.* This starting multitask system can already solve a set of 69 image classification tasks. With *task-set A* we refer to that first set of 69 tasks. With *task-set B* we refer to an additional set of 55 image classification tasks that will be introduced in following experiments.

The continual extension of the system is described as a sequence of experiment segments. Each segment introduces extensions to the method or task-set. The effects on the system in terms of quality, efficiency and capabilities are measured through additional task iterations.

### 5.1 EXPERIMENT SEGMENT 1: $\mu$ 2NET CONVERGENCE

The first experiment segment applies the  $\mu$ 2Net method as defined in (Gesmundo & Dean, 2022b) for an additional number of tasks iterations with the aim of achieving a sufficient system stability and convergence on task-set A. Achieving convergence with the baseline method before transitioning to an extended version allows to attribute the effects observed the following experiment segments to the corresponding method extensions, as the method extensions are compared sequentially rather with standard parallel experiments.

We observe that 2 additional task iterations are required for  $\mu$ 2Net to achieve sufficient convergence on task-set A (see Figure 3). During the first task iteration, the average test accuracy increases by 0.18%. While during the second task iteration, the test accuracy does not improve. The trend of the "average accounted parameters per task" metric is similar, as the variation is significantly smaller during the second iteration. Notice that all the models generated by the  $\mu$ 2Net method have a constant compute cost, that matches the compute cost of the used ViT Large root model with input image resolution of  $384 \times 384$  pixels. This is the case since the  $\mu$ 2Net method does not provide mutation actions that can alter the compute cost of the generated model, such as adding/removing transformer layers or changing the image resolution.

## 5.2 EXPERIMENT SEGMENT 2: $\mu$ 2NET+ INTRODUCTION

The second experiment segment introduces the proposed  $\mu$ 2Net+ method. To produce mild size and compute cost penalties, the scoring function parameters  $P$  and  $F$  are set respectively to  $\sim 10$  times the accounted parameters and inference flops averaged across all the models that are part of the system at the beginning of this experiment segment:  $P = 2.2 \times 10^9$  and  $F = 3.8 \times 10^{12}$ .  $s$  is set to 0.99. All the common evolutionary agents meta parameters, such as those determining the compute utilized per model training and exploratory budget per task iteration, are unchanged for comparability (Gesmundo & Dean, 2022b).

Two additional task iterations on the task-set A are performed. The metrics reported in Figure 3 show that the introduction of the novel method leads the newly generated models to share more parameters and be more computationally efficient. Despite this, the average test quality does not deteriorate. Overall resulting in a 3.6% reduction in compute and 21.7% reduction in size with no loss in quality.

This efficiency improvement is enabled by: 1) the generation of cheaper models is enabled by the introduction of mutation actions allowing to reduce the number of transformer layers and the extension of the hyperparameter search space allowing to chose smaller input image resolution, 2) cheaper models selection is encouraged by the introduction of the size and compute cost factors. 3) the learning process of the  $\mu(\cdot)$  function increases the probability of sampling cheaper models by customizing the probability of occurrence of different mutation types. For example, the probability of performing a layer cloning action decreases from 21.4% to 17.4%, thus decreasing the expected accounted parameter cost of newly sampled models. Furthermore, the learned  $\mu(\cdot)$  functions appear to assign lower cloning probability to lower layers in average (see Figure 6).

## 5.3 EXPERIMENT SEGMENT 3: TASK-SET B INTRODUCTION

The third experiment segment consists in extending the number of jointly solved tasks from 69 to the 124. This is achieved by performing one task iteration on the additional 55 tasks of task-set B to introduce them into the system. These additional image classification tasks are also publicly distributed via the [Tensorflow Datatases catalog](#).

The average test accuracy achieved on task-set B after one task iteration is 90.66%. If we compare to the accuracy achieved at convergence in the next experiment segment (90.78%), we can observe that the system is able to achieve close to converge quality with only one task iteration. While, it took more task iterations to achieve the same relative delta to convergence quality on task-set A: at least 4 task iterations (including the task iteration described in Gesmundo & Dean (2022b)).

This observation can be an empirical evidence supporting the following hypothesis: *The expected convergence time for a new task is inversely proportional to the amount of knowledge embedded in the system.* This hypothesis is based on the intuition that a new task can be learned faster if a model or sub-set or parameters with as relevant knowledge as possible is available to be used or fine-tuned. And the probability for a new task of fining relevant knowledge within the system increases as the system learns more tasks. This hypothesis can be also supported by the sharp drop in "average accounted parameters per task": 14.5% relative reduction during this iteration (see Figure 3), as the new models added to the system seem to take advantage of layers and knowledge sharing with a higher degree.

The average test quality measured on task-set A remains unchanged since its tasks are excluded from this iteration. The average inference compute per task appear to continue to decrease: 4.3% relative reduction in this iteration.

## 5.4 EXPERIMENT SEGMENT 4: $\mu$ 2NET+ CONVERGENCE

To conclude we perform 2 additional task iterations on the union of task-sets A and B.

Interestingly, the average test quality measured on task-set A improves significantly after achieving no significant changes for 3 consecutive task-iterations (see Figure 3). With respect task-set A, the only variation introduced in this experiment segment is the possibility of accessing the new knowledge introduced by learning to solve the additional 55 tasks of task-set B. We measure that, during this experiment segment, 15 tasks of task-set A find an better scoring model by transferring knowledge

from at least one new task of task-set B, and 9 of these improved models transfer knowledge from 2 or more task-set B tasks.

The average inference flops also further improves. Computationally cheaper models are rendered possible by the introduction of the possibility to remove transformer layers and use smaller input image resolutions. Before the introduction of the proposed method all the models used 384 pixels input image resolution and 24 transformer layers as the ViT Large root model. Since the introduction of  $\mu$ 2Net+, 30.4% of the 124 selected models use 224 image resolution, and 27.2% use 23 transformer layers, 1.6% use 22 and 2.4% use 21 transformer layers (see Figure 5).

## 6 CONCLUSION

The reported series of system and method extensions demonstrates the ability of the proposed ML development methodology of integrating the continual design and evaluation process into the unbounded extension of large-scale multitask ML systems. The proposed continual development methodology not only allows for the continual addition of knowledge and tasks into a dynamic multitask system, but also allows for dynamic extensions of the search space defining the architectures and configurations that are possible to explore and furthermore allows to iteratively extend the method exploring such search space while also adapting through time the guiding reward function to adjust according to possibly changing requirements.

Overall, the methodology and empirical results demonstrated in by this work are encouraging signs that a highly automated and incrementally extensible ML system for handling thousands or millions of tasks with improved quality and efficiency is achievable. Future work can continue to build toward a system that can acquire further capabilities and knowledge across multiple modalities.

## REFERENCES

- Jean-Baptiste Alayrac, Jeff Donahue, Pauline Luc, Antoine Miech, Iain Barr, Yana Hasson, Karel Lenc, Arthur Mensch, Katie Millican, Malcolm Reynolds, Roman Ring, Eliza Rutherford, Serkan Cabi, Tengda Han, Zhitao Gong, Sina Samangooei, Marianne Monteiro, Jacob Menick, Sebastian Borgeaud, Andy Brock, Aida Nematzadeh, Sahand Sharifzadeh, Mikolaj Binkowski, Ricardo Barreira, Oriol Vinyals, Andrew Zisserman, and Karen Simonyan. Flamingo: a visual language model for few-shot learning. *ArXiv*, abs/2204.14198, 2022.
- Paul Barham, Aakanksha Chowdhery, Jeffrey Dean, Sanjay Ghemawat, Steven Hand, Daniel Hurt, Michael Isard, Hyeontaek Lim, Ruoming Pang, Sudip Roy, Brennan Saeta, Parker Schuh, Ryan Sepassi, Laurent El Shafey, Chandramohan A. Thekkath, and Yonghui Wu. Pathways: Asynchronous distributed dataflow for ml. *ArXiv*, abs/2203.12533, 2022.
- James Bergstra, Rémi Bardenet, Yoshua Bengio, and Balázs Kégl. Algorithms for hyper-parameter optimization. In *NIPS*, 2011.
- Christopher Berner, Greg Brockman, Brooke Chan, Vicki Cheung, Przemyslaw Debiak, Christy Dennison, David Farhi, Quirin Fischer, Shariq Hashme, Christopher Hesse, Rafal Józefowicz, Scott Gray, Catherine Olsson, Jakub W. Pachocki, Michael Petrov, Henrique Pondé de Oliveira Pinto, Jonathan Raiman, Tim Salimans, Jeremy Schlatter, Jonas Schneider, Szymon Sidor, Ilya Sutskever, Jie Tang, Filip Wolski, and Susan Zhang. Dota 2 with large scale deep reinforcement learning. *ArXiv*, abs/1912.06680, 2019.
- Hakan Bilen, Sylvestre Rebuffi, and Tomas Jakab. Visual domain decathlon. 2017.
- Lukas Bossard, Matthieu Guillaumin, and Luc Van Gool. Food-101 - mining discriminative components with random forests. In *ECCV*, 2014.
- Tom B. Brown, Benjamin Mann, Nick Ryder, Melanie Subbiah, Jared Kaplan, Prafulla Dhariwal, Arvind Neelakantan, Pranav Shyam, Girish Sastry, Amanda Askell, Sandhini Agarwal, Ariel Herbert-Voss, Gretchen Krueger, T. J. Henighan, Rewon Child, Aditya Ramesh, Daniel M. Ziegler, Jeff Wu, Clemens Winter, Christopher Hesse, Mark Chen, Eric Sigler, Mateusz Litwin, Scott Gray, Benjamin Chess, Jack Clark, Christopher Berner, Sam McCandlish, Alec Radford, Ilya Sutskever, and Dario Amodei. Language models are few-shot learners. *ArXiv*, abs/2005.14165, 2020.
- Han Cai, Tianyao Chen, Weinan Zhang, Yong Yu, and Jun Wang. Efficient architecture search by network transformation. In *AAAI*, 2018.
- Tianqi Chen, Ian J. Goodfellow, and Jonathon Shlens. Net2net: Accelerating learning via knowledge transfer. *CoRR*, abs/1511.05641, 2016.
- Zhao Chen, Vijay Badrinarayanan, Chen-Yu Lee, and Andrew Rabinovich. Gradnorm: Gradient normalization for adaptive loss balancing in deep multitask networks. In *ICML*, 2018.
- Gong Cheng, Junwei Han, and Xiaoqiang Lu. Remote sensing image scene classification: Benchmark and state of the art. *Proceedings of the IEEE*, 105:1865–1883, 2017.
- Mircea Cimpoi, Subhansu Maji, Iasonas Kokkinos, Sammy Mohamed, and Andrea Vedaldi. Describing textures in the wild. *2014 IEEE Conference on Computer Vision and Pattern Recognition*, pp. 3606–3613, 2014.
- Tarin Clanuwat, Mikel Bober-Irizar, Asanobu Kitamoto, Alex Lamb, Kazuaki Yamamoto, and David Ha. Deep learning for classical japanese literature. *ArXiv*, abs/1812.01718, 2018.
- Kenneth W. Clark, Bruce A. Vendt, Kirk E. Smith, John B. Freymann, Justin S. Kirby, Paul Koppel, Stephen M. Moore, Stanley R. Phillips, David R. Maffitt, Michael Pringle, Lawrence Tarbox, and Fred W. Prior. The cancer imaging archive (tcia): Maintaining and operating a public information repository. *Journal of Digital Imaging*, 26:1045–1057, 2013.
- Adam Coates, A. Ng, and Honglak Lee. An analysis of single-layer networks in unsupervised feature learning. In *AISTATS*, 2011.

- Gregory Cohen, Saeed Afshar, Jonathan C. Tapson, and André van Schaik. Emnist: Extending mnist to handwritten letters. *2017 International Joint Conference on Neural Networks (IJCNN)*, pp. 2921–2926, 2017.
- N. Das, Jagan Mohan Reddy, Ram Sarkar, Subhadip Basu, Mahantapas Kundu, Mita Nasipuri, and Dipak Kumar Basu. A statistical-topological feature combination for recognition of handwritten numerals. *Appl. Soft Comput.*, 12:2486–2495, 2012a.
- N. Das, Ram Sarkar, Subhadip Basu, Mahantapas Kundu, Mita Nasipuri, and Dipak Kumar Basu. A genetic algorithm based region sampling for selection of local features in handwritten digit recognition application. *Appl. Soft Comput.*, 12:1592–1606, 2012b.
- Jacob Devlin, Ming-Wei Chang, Kenton Lee, and Kristina Toutanova. Bert: Pre-training of deep bidirectional transformers for language understanding. In *NAACL*, 2019.
- Josip Djolonga, Jessica Yung, Michael Tschannen, Rob Romijnders, Lucas Beyer, Alexander Kolesnikov, Joan Puigcerver, Matthias Minderer, Alexander D’Amour, Dan I. Moldovan, Sylvain Gelly, Neil Houlsby, Xiaohua Zhai, and Mario Lucic. On robustness and transferability of convolutional neural networks. *2021 IEEE/CVF Conference on Computer Vision and Pattern Recognition (CVPR)*, pp. 16453–16463, 2021.
- Alexey Dosovitskiy, Lucas Beyer, Alexander Kolesnikov, Dirk Weissenborn, Xiaohua Zhai, Thomas Unterthiner, Mostafa Dehghani, Matthias Minderer, Georg Heigold, Sylvain Gelly, Jakob Uszkoreit, and Neil Houlsby. An image is worth 16x16 words: Transformers for image recognition at scale. *ArXiv*, abs/2010.11929, 2021.
- Nan Du, Yanping Huang, Andrew M. Dai, Simon Tong, Dmitry Lepikhin, Yuanzhong Xu, Maxim Krikun, Yanqi Zhou, Adams Wei Yu, Orhan Firat, Barret Zoph, Liam Fedus, Maarten Bosma, Zongwei Zhou, Tao Wang, Yu Emma Wang, Kellie Webster, Marie Pellat, Kevin Robinson, Kathleen S. Meier-Hellstern, Toju Duke, Lucas Dixon, Kun Zhang, Quoc V. Le, Yonghui Wu, Z. Chen, and Claire Cui. Glam: Efficient scaling of language models with mixture-of-experts. *ArXiv*, abs/2112.06905, 2021.
- Jeremy Elson, John R. Douceur, Jon Howell, and Jared Saul. Asirra: a captcha that exploits interest-aligned manual image categorization. In *CCS ’07*, 2007.
- Li Fei-Fei, Rob Fergus, and Pietro Perona. Learning generative visual models from few training examples: An incremental bayesian approach tested on 101 object categories. 2004.
- Chrisantha Fernando, Dylan S. Banarse, Charles Blundell, Yori Zwols, David R Ha, Andrei A. Rusu, Alexander Pritzel, and Daan Wierstra. Pathnet: Evolution channels gradient descent in super neural networks. *ArXiv*, abs/1701.08734, 2017.
- Robert M. French. Catastrophic forgetting in connectionist networks. *Trends in Cognitive Sciences*, 3:128–135, 1999.
- Andreas Geiger, Philip Lenz, and Raquel Urtasun. Are we ready for autonomous driving? the kitti vision benchmark suite. *2012 IEEE Conference on Computer Vision and Pattern Recognition*, pp. 3354–3361, 2012.
- Andrea Gesmundo and Jeff Dean. munit: Evolving pretrained deep neural networks into scalable auto-tuning multitask systems. *ArXiv*, 2205.10937, 2022a.
- Andrea Gesmundo and Jeff Dean. An evolutionary approach to dynamic introduction of tasks in large-scale multitask learning systems. *ArXiv*, 2205.12755, 2022b.
- David R Ha and Douglas Eck. A neural representation of sketch drawings. *ArXiv*, abs/1704.03477, 2018.
- Kaiming He, X. Zhang, Shaoqing Ren, and Jian Sun. Deep residual learning for image recognition. *2016 IEEE Conference on Computer Vision and Pattern Recognition (CVPR)*, pp. 770–778, 2016.

- Patrick Helber, Benjamin Bischke, Andreas R. Dengel, and Damian Borth. Eurosat: A novel dataset and deep learning benchmark for land use and land cover classification. *IEEE Journal of Selected Topics in Applied Earth Observations and Remote Sensing*, 12:2217–2226, 2019.
- Dan Hendrycks, Steven Basart, Norman Mu, Saurav Kadavath, Frank Wang, Evan Dorundo, Rahul Desai, Tyler Lixuan Zhu, Samyak Parajuli, Mike Guo, Dawn Xiaodong Song, Jacob Steinhardt, and Justin Gilmer. The many faces of robustness: A critical analysis of out-of-distribution generalization. *2021 IEEE/CVF International Conference on Computer Vision (ICCV)*, pp. 8320–8329, 2021a.
- Dan Hendrycks, Kevin Zhao, Steven Basart, Jacob Steinhardt, and Dawn Xiaodong Song. Natural adversarial examples. *2021 IEEE/CVF Conference on Computer Vision and Pattern Recognition (CVPR)*, pp. 15257–15266, 2021b.
- Grant Van Horn, Oisin Mac Aodha, Yang Song, Yin Cui, Chen Sun, Alexander Shepard, Hartwig Adam, Pietro Perona, and Serge J. Belongie. The inaturalist species classification and detection dataset. *2018 IEEE/CVF Conference on Computer Vision and Pattern Recognition*, pp. 8769–8778, 2018.
- Neil Houlsby, Andrei Giurgiu, Stanislaw Jastrzebski, Bruna Morrone, Quentin de Laroussilhe, Andrea Gesmundo, Mona Attariyan, and Sylvain Gelly. Parameter-efficient transfer learning for nlp. In *ICML*, 2019.
- Jeremy Howard. imagenette, 2019a. URL <https://github.com/fastai/imagenette/>.
- Jeremy Howard. Imagemang, 2019b. URL <https://github.com/fastai/imagenette/>.
- David P. Hughes and Marcel Salathé. An open access repository of images on plant health to enable the development of mobile disease diagnostics through machine learning and crowdsourcing. *ArXiv*, abs/1511.08060, 2015.
- Max Jaderberg, Valentin Dalibard, Simon Osindero, Wojciech M. Czarnecki, Jeff Donahue, Ali Razavi, Oriol Vinyals, Tim Green, Iain Dunning, Karen Simonyan, Chrisantha Fernando, and Koray Kavukcuoglu. Population based training of neural networks. *ArXiv*, abs/1711.09846, 2017.
- Lu Jiang, Di Huang, Mason Liu, and Weilong Yang. Beyond synthetic noise: Deep learning on controlled noisy labels. In *ICML*, 2020.
- Justin Johnson, Bharath Hariharan, Laurens van der Maaten, Li Fei-Fei, C. Lawrence Zitnick, and Ross B. Girshick. Clevr: A diagnostic dataset for compositional language and elementary visual reasoning. *2017 IEEE Conference on Computer Vision and Pattern Recognition (CVPR)*, pp. 1988–1997, 2017.
- Norman P. Jouppi, Cliff Young, Nishant Patil, David A. Patterson, Gaurav Agrawal, Raminder Singh Bajwa, Sarah Bates, Suresh Bhatia, Nanette J. Boden, Al Borchers, Rick Boyle, Pierre luc Cantin, Clifford Chao, Chris Clark, Jeremy Coriell, Mike Daley, Matt Dau, Jeffrey Dean, Ben Gelb, Tara Vazir Ghaemmaghami, Rajendra Gottipati, William Gulland, Robert B. Hagmann, C. Richard Ho, Doug Hogberg, John Hu, Robert Hundt, Daniel Hurt, Julian Ibarz, Aaron Jaffey, Alek Jaworski, Alexander Kaplan, Harshit Khaitan, Daniel Killebrew, Andy Koch, Naveen Kumar, Steve Lacy, James Laudon, James Law, Diemthu Le, Chris Leary, Zhuyuan Liu, Kyle A. Lucke, Alan Lundin, Gordon MacKean, Adriana Maggiore, Maire Mahony, Kieran Miller, Rahul Nagarajan, Ravi Narayanaswami, Ray Ni, Kathy Nix, Thomas Norrie, Mark Omernick, Narayana Penukonda, Andy Phelps, Jonathan Ross, Matt Ross, Amir Salek, Emad Samadiani, Chris Severn, Gregory Sizikov, Matthew Snelham, Jed Souter, Dan Steinberg, Andy Swing, Mercedes Tan, Gregory Thorson, Bo Tian, Horia Toma, Erick Tuttle, Vijay Vasudevan, Richard Walter, Walter Wang, Eric Wilcox, and Doe Hyun Yoon. In-datacenter performance analysis of a tensor processing unit. *2017 ACM/IEEE 44th Annual International Symposium on Computer Architecture (ISCA)*, pp. 1–12, 2017.
- Kaggle and EyePacs. Kaggle diabetic retinopathy detection. <https://www.kaggle.com/c/diabetic-retinopathy-detection/data>, 2015.

- Jakob Nikolas Kather, Cleo-Aron Weis, Francesco Bianconi, Susanne Maria Melchers, Lothar Rudi Schad, Timo Gaiser, Alexander Marx, and Frank G. Zöllner. Multi-class texture analysis in colorectal cancer histology. *Scientific Reports*, 6, 2016.
- Alex Kendall, Yarin Gal, and Roberto Cipolla. Multi-task learning using uncertainty to weigh losses for scene geometry and semantics. *2018 IEEE/CVF Conference on Computer Vision and Pattern Recognition*, pp. 7482–7491, 2018.
- Aditya Khosla, Nityananda Jayadevaprakash, Bangpeng Yao, and Li Fei-Fei. Novel dataset for fine-grained image categorization : Stanford dogs. 2012.
- David A. Klindt, Lukas Schott, Yash Sharma, Ivan Ustyuzhaninov, Wieland Brendel, Matthias Bethge, and Dylan M. Paiton. Towards nonlinear disentanglement in natural data with temporal sparse coding. *ArXiv*, abs/2007.10930, 2021.
- Efi Kokkiopoulou, Anja Hauth, Luciano Sbaiz, Andrea Gesmundo, Gábor Bartók, and Jesse Berent. Fast task-aware architecture inference. *ArXiv*, abs/1902.05781, 2019.
- Vippon Preet Kour and Sakshi Arora. Plantaek: A leaf database of native plants of jammu and kashmir. 2019.
- Jonathan Krause, Michael Stark, Jia Deng, and Li Fei-Fei. 3d object representations for fine-grained categorization. *2013 IEEE International Conference on Computer Vision Workshops*, pp. 554–561, 2013.
- Alex Krizhevsky. Learning multiple layers of features from tiny images. 2009.
- Brenden M. Lake, Ruslan Salakhutdinov, and Joshua B. Tenenbaum. Human-level concept learning through probabilistic program induction. *Science*, 350:1332 – 1338, 2015.
- Yann LeCun, Léon Bottou, Yoshua Bengio, and Patrick Haffner. Gradient-based learning applied to document recognition. *Proc. IEEE*, 86:2278–2324, 1998.
- Yann LeCun, Fu Jie Huang, and Léon Bottou. Learning methods for generic object recognition with invariance to pose and lighting. *Proceedings of the 2004 IEEE Computer Society Conference on Computer Vision and Pattern Recognition, 2004. CVPR 2004.*, 2:II–104 Vol.2, 2004.
- Hanxiao Liu, Karen Simonyan, and Yiming Yang. Darts: Differentiable architecture search. *ArXiv*, abs/1806.09055, 2019a.
- Shengchao Liu, Yingyu Liang, and Anthony Gitter. Loss-balanced task weighting to reduce negative transfer in multi-task learning. In *AAAI*, 2019b.
- Ziwei Liu, Zhongqi Miao, Xiaohang Zhan, Jiayun Wang, Boqing Gong, and Stella X. Yu. Large-scale long-tailed recognition in an open world. *2019 IEEE/CVF Conference on Computer Vision and Pattern Recognition (CVPR)*, pp. 2532–2541, 2019c.
- AI Lab Makerere. Bean disease dataset, January 2020. URL <https://github.com/AI-Lab-Makerere/ibean>.
- Krzysztof Maziarsz, Andrey Khorlin, Quentin de Laroussilhe, and Andrea Gesmundo. Evolutionary-neural hybrid agents for architecture search. *ArXiv*, abs/1811.09828, 2018.
- Michael McCloskey and Neal J. Cohen. Catastrophic interference in connectionist networks: The sequential learning problem. *Psychology of Learning and Motivation*, 24:109–165, 1989.
- Thomas Mensink, Jasper R. R. Uijlings, Alina Kuznetsova, Michael Gygli, and Vittorio Ferrari. Factors of influence for transfer learning across diverse appearance domains and task types. *IEEE transactions on pattern analysis and machine intelligence*, PP, 2021.
- Laurence Moroney. Horses or humans dataset, feb 2019a. URL <http://laurencemoroney.com/horses-or-humans-dataset>.
- Laurence Moroney. Rock, paper, scissors dataset, 2019b. URL <http://laurencemoroney.com/rock-paper-scissors-dataset>.

- Ernest Mwebaze, Timnit Gebru, Andrea Frome, Solomon Nsumba, and Tusubira Francis Jeremy. icassava 2019 fine-grained visual categorization challenge. *ArXiv*, abs/1908.02900, 2019.
- Yuval Netzer, Tao Wang, Adam Coates, A. Bissacco, Bo Wu, and A. Ng. Reading digits in natural images with unsupervised feature learning. 2011.
- Maria-Elena Nilsback and Andrew Zisserman. Automated flower classification over a large number of classes. *2008 Sixth Indian Conference on Computer Vision, Graphics & Image Processing*, pp. 722–729, 2008.
- Alex Olsen, Dmitry A. Konovalov, Bronson W Philippa, Peter V. Ridd, Jake C. Wood, Jamie Johns, Wesley Banks, Benjamin Girgenti, Owen Kenny, James C. Whinney, Brendan Calvert, Mostafa Rahimi Azghadi, and Ronald D. White. Deepweeds: A multiclass weed species image dataset for deep learning. *Scientific Reports*, 9, 2019.
- Omkar M. Parkhi, Andrea Vedaldi, Andrew Zisserman, and C. V. Jawahar. Cats and dogs. *2012 IEEE Conference on Computer Vision and Pattern Recognition*, pp. 3498–3505, 2012.
- Xingchao Peng, Qinxun Bai, Xide Xia, Zijun Huang, Kate Saenko, and Bo Wang. Moment matching for multi-source domain adaptation. *2019 IEEE/CVF International Conference on Computer Vision (ICCV)*, pp. 1406–1415, 2019.
- Hieu Pham, Melody Y. Guan, Barret Zoph, Quoc V. Le, and Jeff Dean. Efficient neural architecture search via parameter sharing. In *ICML*, 2018.
- Colin Raffel, Noam M. Shazeer, Adam Roberts, Katherine Lee, Sharan Narang, Michael Matena, Yanqi Zhou, Wei Li, and Peter J. Liu. Exploring the limits of transfer learning with a unified text-to-text transformer. *ArXiv*, abs/1910.10683, 2020.
- Sivaramakrishnan Rajaraman, Sameer Kiran Antani, Mahdieh Poostchi, Kamolrat Silamut, Md Amir Hossain, Richard James Maude, Stefan Jaeger, and George R. Thoma. Pre-trained convolutional neural networks as feature extractors toward improved malaria parasite detection in thin blood smear images. *PeerJ*, 6, 2018.
- Rahul Ramesh and Pratik Chaudhari. Model zoo: A growing brain that learns continually. In *ICLR*, 2022.
- Hafiz Tayyab Rauf, Basharat Ali Saleem, Muhammad Ikram Ullah Lali, Muhammad Attique Khan, Muhammad Usman Sharif, and Syed Ahmad Chan Bukhari. A citrus fruits and leaves dataset for detection and classification of citrus diseases through machine learning. *Data in Brief*, 26, 2019.
- Esteban Real, Alok Aggarwal, Yanping Huang, and Quoc V. Le. Regularized evolution for image classifier architecture search. In *AAAI*, 2019.
- Sylvestre-Alvise Rebuffi, Hakan Bilen, and Andrea Vedaldi. Learning multiple visual domains with residual adapters. In *NIPS*, 2017.
- Scott Reed, Konrad Zolna, Emilio Parisotto, Sergio Gomez Colmenarejo, Alexander Novikov, Gabriel Barth-Maron, Mai Gimenez, Yury Sulsky, Jackie Kay, Jost Tobias Springenberg, Tom Eccles, Jake Bruce, Ali Razavi, Ashley D. Edwards, Nicolas Manfred Otto Heess, Yutian Chen, Raia Hadsell, Oriol Vinyals, Mahyar Bordbar, and Nando de Freitas. A generalist agent. *ArXiv*, abs/2205.06175, 2022.
- Amir Rosenfeld and John K. Tsotsos. Incremental learning through deep adaptation. *IEEE Transactions on Pattern Analysis and Machine Intelligence*, 42:651–663, 2020.
- Michael T. Rosenstein. To transfer or not to transfer. In *NIPS 2005*, 2005.
- Olga Russakovsky, Jia Deng, Hao Su, Jonathan Krause, Sanjeev Satheesh, Sean Ma, Zhiheng Huang, Andrej Karpathy, Aditya Khosla, Michael S. Bernstein, Alexander C. Berg, and Li Fei-Fei. Imagenet large scale visual recognition challenge. *International Journal of Computer Vision*, 115: 211–252, 2015.

- Andrei A. Rusu, Neil C. Rabinowitz, Guillaume Desjardins, Hubert Soyer, James Kirkpatrick, Koray Kavukcuoglu, Razvan Pascanu, and Raia Hadsell. Progressive neural networks. *ArXiv*, abs/1606.04671, 2016.
- Ozan Sener and Vladlen Koltun. Multi-task learning as multi-objective optimization. In *NeurIPS*, 2018.
- Noam M. Shazeer, Azalia Mirhoseini, Krzysztof Maziarz, Andy Davis, Quoc V. Le, Geoffrey E. Hinton, and Jeff Dean. Outrageously large neural networks: The sparsely-gated mixture-of-experts layer. *ArXiv*, abs/1701.06538, 2017.
- Jasper Snoek, H. Larochelle, and Ryan P. Adams. Practical bayesian optimization of machine learning algorithms. In *NIPS*, 2012.
- Hyun Oh Song, Yu Xiang, Stefanie Jegelka, and Silvio Savarese. Deep metric learning via lifted structured feature embedding. *2016 IEEE Conference on Computer Vision and Pattern Recognition (CVPR)*, pp. 4004–4012, 2016.
- Niranjan Srinivas, Andreas Krause, Sham M. Kakade, and Matthias W. Seeger. Gaussian process optimization in the bandit setting: No regret and experimental design. In *ICML*, 2010.
- Andreas Steiner, Alexander Kolesnikov, Xiaohua Zhai, Ross Wightman, Jakob Uszkoreit, and Lucas Beyer. How to train your vit? data, augmentation, and regularization in vision transformers. *ArXiv*, abs/2106.10270, 2021.
- Yu Sun, Shuohuan Wang, Yukun Li, Shikun Feng, Hao Tian, Hua Wu, and Haifeng Wang. Ernie 2.0: A continual pre-training framework for language understanding. *ArXiv*, abs/1907.12412, 2020.
- Mingxing Tan, Bo Chen, Ruoming Pang, Vijay Vasudevan, and Quoc V. Le. Mnasnet: Platform-aware neural architecture search for mobile. *2019 IEEE/CVF Conference on Computer Vision and Pattern Recognition (CVPR)*, pp. 2815–2823, 2019.
- Romal Thoppilan, Daniel De Freitas, Jamie Hall, Noam M. Shazeer, Apoorv Kulshreshtha, Heng-Tze Cheng, Alicia Jin, Taylor Bos, Leslie Baker, Yu Du, Yaguang Li, Hongrae Lee, Huaixiu Zheng, Amin Ghafouri, Marcelo Menegali, Yanping Huang, Maxim Krikun, Dmitry Lepikhin, James Qin, Dehao Chen, Yuanzhong Xu, Zhifeng Chen, Adam Roberts, Maarten Bosma, Yanqi Zhou, Chung-Ching Chang, I. A. Krivokon, Willard James Rusch, Marc Pickett, Kathleen S. Meier-Hellstern, Meredith Ringel Morris, Tulse Doshi, Renelito Delos Santos, Toju Duke, Johnny Hartz Søraker, Ben Zevenbergen, Vinodkumar Prabhakaran, Mark Diaz, Ben Hutchinson, Kristen Olson, Alejandra Molina, Erin Hoffman-John, Josh Lee, Lora Aroyo, Ravindran Rajakumar, Alena Butryna, Matthew Lamm, V. O. Kuzmina, Joseph Fenton, Aaron Cohen, Rachel Bernstein, Ray Kurzweil, Blaise Aguera-Arcas, Claire Cui, Marian Croak, Ed Chi, and Quoc Le. Lamda: Language models for dialog applications. *ArXiv*, abs/2201.08239, 2022.
- Bastiaan S. Veeling, Jasper Linmans, Jim Winkens, Taco Cohen, and Max Welling. Rotation equivariant cnns for digital pathology. *ArXiv*, abs/1806.03962, 2018.
- Haohan Wang, Songwei Ge, Eric P. Xing, and Zachary Chase Lipton. Learning robust global representations by penalizing local predictive power. In *NeurIPS*, 2019a.
- Zirui Wang, Zihang Dai, Barnabás Póczos, and Jaime G. Carbonell. Characterizing and avoiding negative transfer. *2019 IEEE/CVF Conference on Computer Vision and Pattern Recognition (CVPR)*, pp. 11285–11294, 2019b.
- Peter Welinder, Steve Branson, Takeshi Mita, Catherine Wah, Florian Schroff, Serge J. Belongie, and Pietro Perona. Caltech-ucsd birds 200. 2010.
- Jianxiong Xiao, James Hays, Krista A. Ehinger, Aude Oliva, and Antonio Torralba. Sun database: Large-scale scene recognition from abbey to zoo. *2010 IEEE Computer Society Conference on Computer Vision and Pattern Recognition*, pp. 3485–3492, 2010.
- Yi Yang and S. Newsam. Bag-of-visual-words and spatial extensions for land-use classification. In *GIS '10*, 2010.

- Jaehong Yoon, Eunho Yang, Jeongtae Lee, and Sung Ju Hwang. Lifelong learning with dynamically expandable networks. *ArXiv*, abs/1708.01547, 2018.
- Tianhe Yu, Saurabh Kumar, Abhishek Gupta, Sergey Levine, Karol Hausman, and Chelsea Finn. Gradient surgery for multi-task learning. *ArXiv*, abs/2001.06782, 2020.
- Xiaohua Zhai, Joan Puigcerver, Alexander Kolesnikov, Pierre Ruysen, Carlos Riquelme, Mario Lucic, Josip Djolonga, André Susano Pinto, Maxim Neumann, Alexey Dosovitskiy, Lucas Beyer, Olivier Bachem, Michael Tschannen, Marcin Michalski, Olivier Bousquet, Sylvain Gelly, and Neil Houlsby. The visual task adaptation benchmark. *ArXiv*, abs/1910.04867, 2019.
- Jun Zhang, Zhi hui Zhan, Ying Lin, Ni Chen, Yue jiao Gong, Jinghui Zhong, Henry Shu hung Chung, Yun Li, and Yu hui Shi. Evolutionary computation meets machine learning: A survey. *IEEE Computational Intelligence Magazine*, 6:68–75, 2011.
- Wen Zhang, Lingfei Deng, Lei Zhang, and Dongrui Wu. A survey on negative transfer. 2020.
- Bolei Zhou, Àgata Lapedriza, Aditya Khosla, Aude Oliva, and Antonio Torralba. Places: A 10 million image database for scene recognition. *IEEE Transactions on Pattern Analysis and Machine Intelligence*, 40:1452–1464, 2018.
- Jun-Yan Zhu, Taesung Park, Phillip Isola, and Alexei A. Efros. Unpaired image-to-image translation using cycle-consistent adversarial networks. *2017 IEEE International Conference on Computer Vision (ICCV)*, pp. 2242–2251, 2017.
- Barret Zoph and Quoc V. Le. Neural architecture search with reinforcement learning. *ArXiv*, abs/1611.01578, 2017.

## A EXTENDED RELATED WORK SURVEY

The proposed method is designed to learn a unbounded number of tasks in a continual learning fashion. In such contexts it aims to learn each task with higher quality and efficiency by automating and optimizing the knowledge transfer among any subset of tasks that can provide useful knowledge to one another. The proposed model is designed to be immune from common multitask learning pitfalls: catastrophic forgetting, gradients interference, negative transfer. Cross-task **transfer-learning** has gained popularity, especially through transfer learning from a model pre-trained on a large amount of data for one or a few general tasks, and then fine-tuned on a small amount of data for a related downstream task. This approach has been shown to be very effective in a wide variety of problems across many modalities, including language (Devlin et al., 2019; Raffel et al., 2020) and vision (Dosovitskiy et al., 2021; He et al., 2016). The success of transfer-learning applications hinges on adequate prior knowledge selection to avoid typical negative-transfer pitfalls (Rosenstein, 2005; Wang et al., 2019b). Common solutions rely on data or model selection techniques, often putting emphasis on the efficiency of the exploration (Zhang et al., 2020; Mensink et al., 2021). Transfer learning capabilities are critical for **multitask models**. ML models trained jointly on multiple tasks can be affected by gradients interference if any subset of parameters receive gradients jointly from multiple sources (Chen et al., 2018; Yu et al., 2020), and by catastrophic forgetting of prior knowledge as new tasks are learned (McCloskey & Cohen, 1989; French, 1999). These knowledge loss problems can be alleviated with weighted combination of tasks (Liu et al., 2019b; Sun et al., 2020) and gradient transformation methods (Chen et al., 2018; Sener & Koltun, 2018; Kendall et al., 2018). Stronger guarantees are provided by methods that compartmentalize task specific knowledge in dedicated parameter subsets (Rebuffi et al., 2017; Houlsby et al., 2019; Rusu et al., 2016; Rosenfeld & Tsotsos, 2020). Addressing catastrophic forgetting and identifying what subset of parameters/knowledge that is beneficial to share with each task is also critical for **continual learning** or life long learning methods (McCloskey & Cohen, 1989; French, 1999; Ramesh & Chaudhari, 2022).

The proposed method relies on an evolutionary approach to jointly search the spaces of models architectures, hyperparameters, and prior knowledge selection while optimizing for an possibly multi-factor non-differentiable reward function. The automation of **hyperparameter tuning** has been commonly addressed with Bayesian optimization (Srinivas et al., 2010; Bergstra et al., 2011; Snoek et al., 2012), evolutionary methods have also been explored for this purpose (Jaderberg et al., 2017; Zhang et al., 2011). Hyperparameters tuning can be considered related to the **neural architecture search** (NAS), as architectures can be defined by the selection of a sequence of architectural hyperparameters. Initially, NAS methods have been based on reinforcement learning techniques (Zoph & Le, 2017) but also sample efficient evolutionary approaches have also proposed (Real et al., 2019; Maziarz et al., 2018). Alternative NAS methods focusing on more efficient parameter-sharing (Pham et al., 2018; Liu et al., 2019a; Kokiopoulou et al., 2019) or optimization for multi-factor quality/cost trade-offs (Tan et al., 2019) have also been explored.

The proposed method is capable to dynamically extend the system, adding capacity or novel structures in an unconstrained fashion. A large amount of methods have been proposed to achieve **dynamic architecture extensions** (Chen et al., 2016), some also focusing on an unbounded stream of tasks (Yoon et al., 2018), or achieving immunity from catastrophic forgetting (Rusu et al., 2016; Rosenfeld & Tsotsos, 2020).

The proposed method is sparsely activated, thus the unbounded growth of knowledge and parameters is decoupled from the growth of computational cost. Commonly, **sparse activation** techniques can be defined at sub-layer level (Shazeer et al., 2017; Du et al., 2021) or network route level (Fernando et al., 2017).

## B EXPERIMENTS DETAILS

All the experiments reported in this paper can be reproduced by using the following public resources:

- The published code of the proposed  $\mu$ 2Net+: <https://github.com/google-research/google-research/tree/master/muNet>
- $\mu$ 2Net and the large scale model checkpoint: <https://github.com/google-research/google-research/tree/master/muNet>
- The ViT model definition and checkpoints published by Steiner et al. (2021). These resources are available at [https://github.com/google-research/vision\\_transformer](https://github.com/google-research/vision_transformer) and distributed under the [Apache License 2.0](#).
- All the 124 datasets are publicly available via the Tensorflow Datasets image classification, catalog. Refer to <https://www.tensorflow.org/datasets/catalog/overview> for detailed information regarding each dataset licence and other metadata. Table 4 reports dataset splits used for the experiments and reference for each task.

We also publish the  $\mu$ 2Net+ checkpoint resulting from the large-scale multitask experiment reported in Section 5. This checkpoint can be used for inference on any of the 124 learned image classification tasks, or for further analysis, or even to be extended with additional tasks or methods. For information about the checkpoint and its license refer to: <https://github.com/google-research/google-research/tree/master/muNet>

The experiments reported in Sections 4 have been executed on a TPUv3 (Jouppi et al., 2017) machine with 8 cores. While, the large scale experiments reported in Section 5 have been executed on a larger scale infrastructure using 32 TPUv4 chips in MegaCore mode, by using the Pathways orchestration layer (Barham et al., 2022), to accommodate for the increased memory requirements and scale.

Table 3: Video representation of evolution of the large scale multitask system extended by each of the experiment segment described in Section 5

Segment	Video
1: $\mu$ 2Net 2 task iterations on task-set A	<a href="https://youtu.be/hDDCMpfCJ3s">https://youtu.be/hDDCMpfCJ3s</a>
2: $\mu$ 2Net+ 2 task iterations on task-set A	<a href="https://youtu.be/tf5tzuxbxx8">https://youtu.be/tf5tzuxbxx8</a>
3: $\mu$ 2Net+ 1 task iteration to add task-set B	<a href="https://youtu.be/jGkzXE2WLV0">https://youtu.be/jGkzXE2WLV0</a>
4: $\mu$ 2Net+ 2 task iterations on task-set A+B	<a href="https://youtu.be/CW_BAwkQ9e8">https://youtu.be/CW_BAwkQ9e8</a>

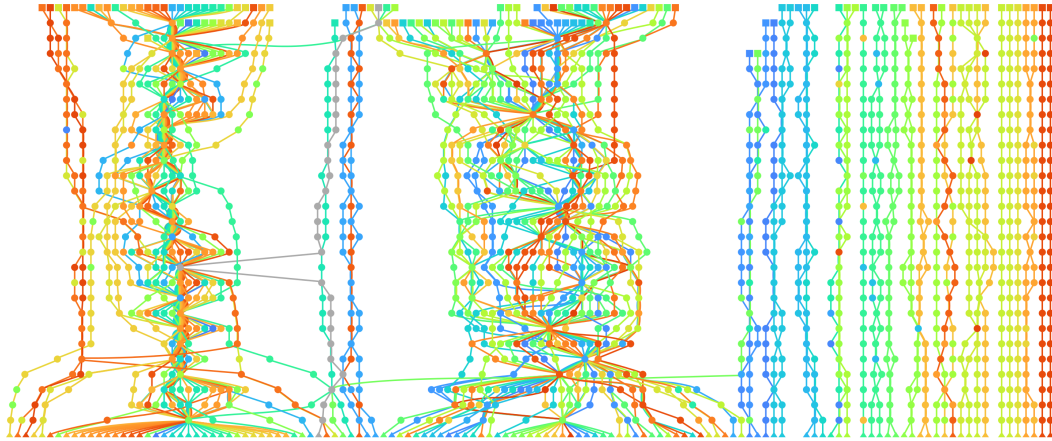


Figure 4: Graph representing the architecture of the multitask system solving jointly 124 image classification tasks generated by the large scale continual learning experiments described in Section 5. Each task is identified with a unique color. Bottom triangular nodes represent the data input of each task. Top rectangular nodes represent the head layer of each task. Each edges sequence of the same color connecting a task input to its head defines the layers sequence composing the model for each task. Each path traverses a sequence of round nodes representing ViT L/16 internal layers in the following order from bottom to top: patch embedding, class token, position embedding and a variable number of transformer layers. Internal nodes are represented with the color of the task on which the parameters of the corresponding layer were trained last. Except for the gray nodes that have not received gradient updates from any of the 124 tasks and still carry the parameters of the root model that was loaded from a checkpoint of the ViT Large model pretrained on the imagenet-21k dataset as described by Gesmundo & Dean (2022b). See Table 3 for animations of the evolutionary process. The structure displays the formation of two main clusters of models/paths having a high degree of layers sharing. These are models selected for tasks that can achieve peak quality with a lower degree of knowledge specialization. Few models form smaller and disconnected clusters of paths. Notice that knowledge sharing is effective even for models/paths that result in a disconnected sub-graph, since ancestors models may have been trained on multiple tasks whose current best model has fully branched in a separate disconnected structure during the evolutionary process. Among these small clusters it is visible a high degree of sharing among related tasks. For example, the leftmost disconnected subgraph of 3 paths contains only characters classification tasks: *bangla*, *devanagari* and *binary\_alpha\_digits* (see Table 4 for datasets details). The majority of the disconnected subgraphs of 2 paths contain each a VTAB-Full task paired with the matching VTAB-1k "few-shots learning" version of the same task, from left to right: 1) *clevr/count\_all* and *clevr/count\_all<sub>1k</sub>*, 2) *dmlab* and *dmlab<sub>1k</sub>*, 3) *dsprites/label\_orientation* and *dsprites/label\_orientation<sub>1k</sub>*, 4) *eurosat* and *eurosat<sub>1k</sub>*, 5) *resisc45* and *resisc45<sub>1k</sub>*, 6) *smallnorb/label\_azimuth* and *smallnorb/label\_azimuth<sub>1k</sub>*.

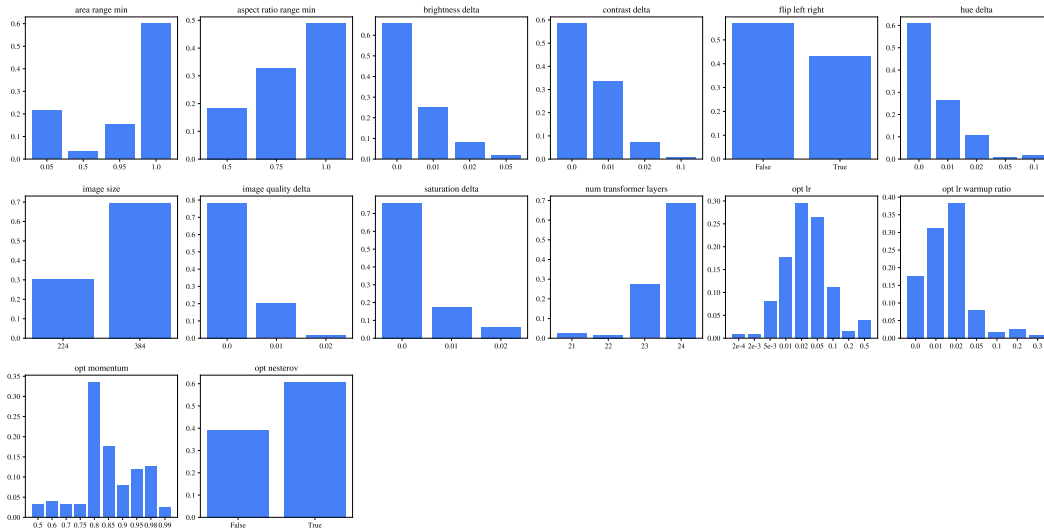


Figure 5: Distributions of the hyperparameter values used by the 124 models included in the multitask system at the end of the sequence of experiments described in Section 5.

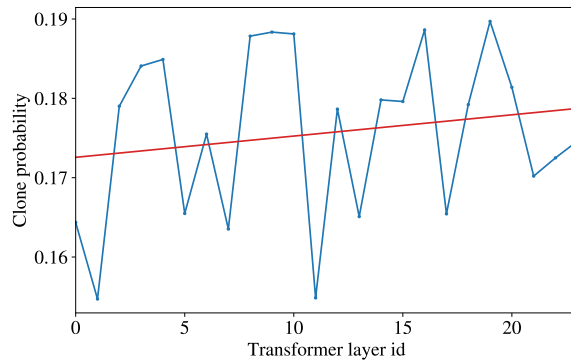


Figure 6: Displays the mutation probabilities learned by the  $\mu$  function for cloning transformer layers at different depth, lower layer ids correspond to transformer layers closer to the model input. The displayed mutation probabilities are averaged across the values learned by the  $\mu$  functions learned for the 124 models included in the multitask system at the end of the sequence of experiments described in Section 5. The red line is fitted to minimize the squared distance to the curve.

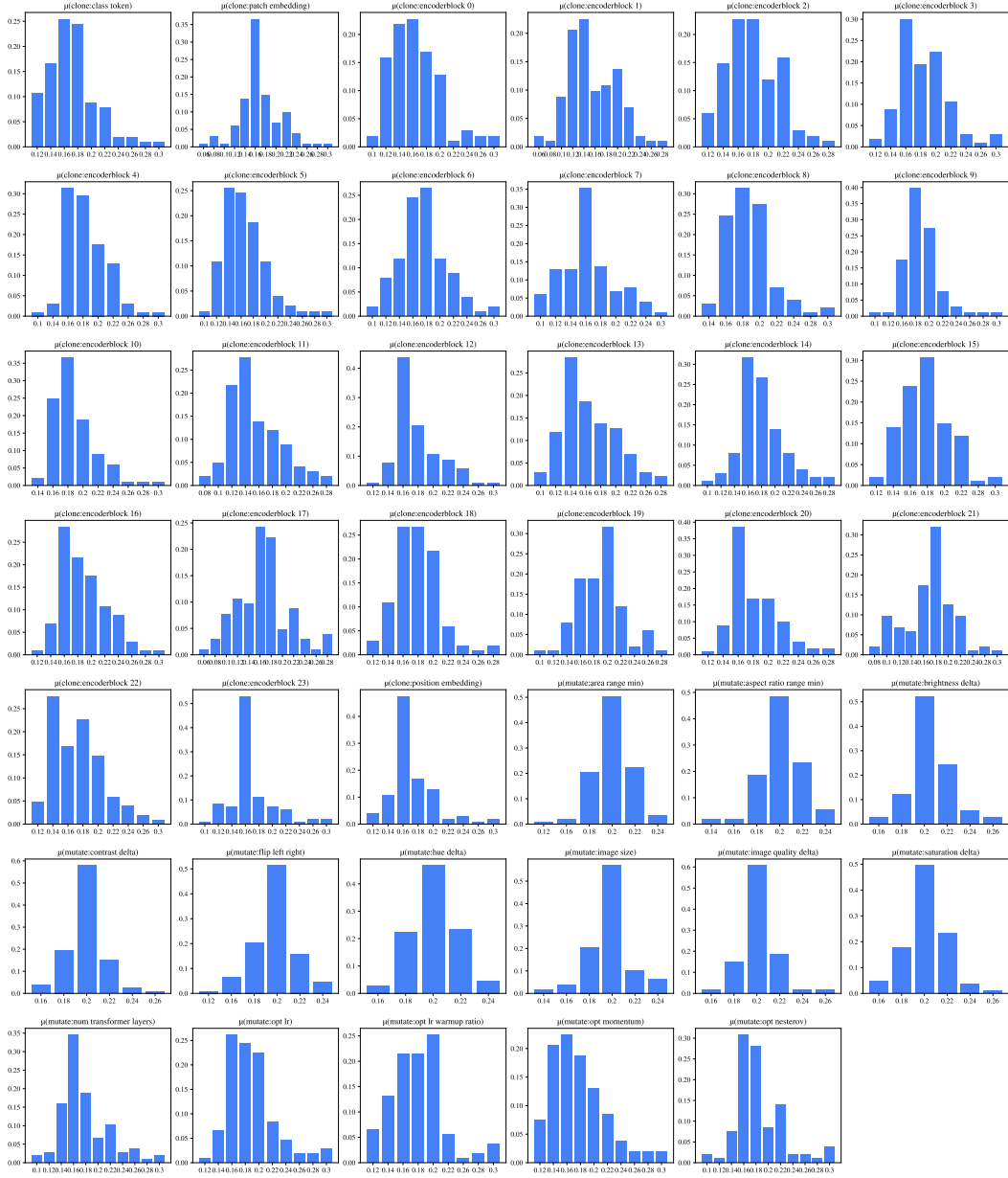


Figure 7: Distributions of the  $\mu(\cdot)$  values conditioned on different mutations of hyperparameters and clonable layers. The histograms aggregates the values of the 124 models included in the multitask system at the end of the sequence of experiments described in Section 5.

Table 4: Datasets details (part 1 of 3). For each dataset used in the experiments, this table reports: 1) accuracy achieved on the test and validations sets by the large scale multitask model generated by the experiments described in Section 5 2) dataset name indicative of the Tensorflow Datasets Catalogs identification string and linking to the corresponding catalog page, 3) train, validation and test data splits, represented with the [standard Tensorflow Datasets format](#) ("validation" has been abbreviated as "val"). 4) corresponding scientific publication reference. Datasets are listed in the order of introduction into the system.

Notes:

[1] The test split of the [imagenet\\_v2](#) dataset is used as validation set for [imagenet2012](#).

[2] The test split of the [cifar10\\_1](#) dataset is used as validation set for [cifar10](#).

[3] The VTAB-full benchmark also includes the cifar100 task. Cifar100 has been introduced to the system as part of the initial benchmark. In the VTAB-full results tables we refer to the top 1 test accuracy achieved in the latest cifar100 training iteration without retraining it as part of the VTAB-full active training iteration.

[4] The definition for the VTAB standard and additional tasks has been sourced from [https://github.com/google-research/task\\_adaptation/tree/master/task\\_adaptation/data](https://github.com/google-research/task_adaptation/tree/master/task_adaptation/data).

[5] VTAB additional task, not included in the standard scoring set. These tasks were added to further scale the system and analyze transfer across related tasks.

Name	Accuracy (%)		Splits			Reference
	Val.	Test	Train	Val.	Test	
<b>Task-set A</b>						
<a href="#">imagenet2012</a>	78.54	86.66	train	<a href="#">imagenet_v2:test</a> <sup>[1]</sup>	val	(Russakovsky et al., 2015)
<a href="#">cifar100</a>	96.88	94.94	<a href="#">train[:98%]</a>	<a href="#">train[98%:]</a>	test	(Krizhevsky, 2009)
<a href="#">cifar10</a>	98.81	99.48	train	<a href="#">cifar10_1:test</a> <sup>[2]</sup>	test	(Krizhevsky, 2009)
VTAB-full benchmark <sup>[3][4]</sup>						
<a href="#">caltech101</a>	98.67	95.94	<a href="#">train[:2754]</a>	<a href="#">train[2754:]</a>	test	(Fei-Fei et al., 2004)
<a href="#">dtd</a>	82.63	82.23	train	val	test	(Cimpoi et al., 2014)
<a href="#">oxford_flowers102</a>	99.79	99.48	train	val	test	(Nilsback & Zisserman, 2008)
<a href="#">oxford_iiit_pet</a>	98.09	95.50	<a href="#">train[:2944]</a>	<a href="#">train[2944:]</a>	test	(Parkhi et al., 2012)
<a href="#">sun397</a>	84.71	84.32	train	val	test	(Xiao et al., 2010)
<a href="#">svhn_cropped</a>	97.47	97.50	<a href="#">train[:65931]</a>	<a href="#">train[65931:]</a>	test	(Netzer et al., 2011)
<a href="#">patch_camelyon</a>	92.82	91.14	train	val	test	(Veeling et al., 2018)
<a href="#">eurosat/rgb</a>	99.27	99.22	<a href="#">train[:16200]</a>	<a href="#">train[16200:21600]</a>	<a href="#">train[21600:]</a>	(Helber et al., 2019)
<a href="#">resisc45</a>	97.80	97.21	<a href="#">train[:18900]</a>	<a href="#">train[18900:25200]</a>	<a href="#">train[25200:]</a>	(Cheng et al., 2017)
<a href="#">diabetic_retinopathy_detection/...</a>						
<a href="#">btgraham-300</a>	85.22	83.75	train	val	test	(Kaggle & EyePacs, 2015)
<a href="#">clevr/count_cylinders</a> <sup>[5]</sup>	99.65	99.47	<a href="#">train[:63000]</a>	<a href="#">train[63000:]</a>	val	(Johnson et al., 2017)
<a href="#">clevr/count_all</a>	99.97	99.90	<a href="#">train[:63000]</a>	<a href="#">train[63000:]</a>	val	(Johnson et al., 2017)
<a href="#">clevr/closest_object_distance</a>	94.63	94.05	<a href="#">train[:63000]</a>	<a href="#">train[63000:]</a>	val	(Johnson et al., 2017)
<a href="#">dmlab</a>	77.01	76.92	train	val	test	(Zhai et al., 2019)
<a href="#">dsprites/label_x_position</a>	99.99	99.98	<a href="#">train[:589824]</a>	<a href="#">train[589824:663552]</a>	<a href="#">train[663552:]</a>	(Klindt et al., 2021)
<a href="#">dsprites/label_orientation</a>	96.78	96.44	<a href="#">train[:589824]</a>	<a href="#">train[589824:663552]</a>	<a href="#">train[663552:]</a>	(Klindt et al., 2021)
<a href="#">kitti/closest_object_distance</a> <sup>[5]</sup>	83.57	78.48	train	val	test	(Geiger et al., 2012)
<a href="#">kitti/count_vehicles</a> <sup>[5]</sup>	92.14	76.93	train	val	test	(Geiger et al., 2012)
<a href="#">kitti/closest_vehicle_distance</a>	89.76	82.28	train	val	test	(Geiger et al., 2012)
<a href="#">smallnorb/label_category</a> <sup>[5]</sup>	99.45	99.38	train	<a href="#">test[:50%]</a>	<a href="#">test[50%:]</a>	(LeCun et al., 2004)
<a href="#">smallnorb/label_lighting</a> <sup>[5]</sup>	99.93	99.89	train	<a href="#">test[:50%]</a>	<a href="#">test[50%:]</a>	(LeCun et al., 2004)
<a href="#">smallnorb/label_azimuth</a>	35.40	34.44	train	<a href="#">test[:50%]</a>	<a href="#">test[50%:]</a>	(LeCun et al., 2004)
<a href="#">smallnorb/label_elevation</a>	96.22	96.26	train	<a href="#">test[:50%]</a>	<a href="#">test[50%:]</a>	(LeCun et al., 2004)

Continues in Table 5 . . .

Table 5: Datasets details (part 2 of 3).

Name	Accuracy (%)		Splits			Reference
	Val.	Test	Train	Val.	Test	
... Continues from Table 4						
Visual domain decathlon benchmark						
visual_domain_decathlon/...						
imagenet12	89.47	89.69	train	val[:50%]	val[50%:]	(Bilen et al., 2017)
svhn	98.75	98.57	train	val[:50%]	val[50%:]	(Bilen et al., 2017)
cifar100	97.79	98.00	train	val[:50%]	val[50%:]	(Bilen et al., 2017)
gtsrb	100	99.95	train	val[:50%]	val[50%:]	(Bilen et al., 2017)
daimlerpedcls	100	100	train	val[:50%]	val[50%:]	(Bilen et al., 2017)
omniglot	88.70	87.99	train	val[:50%]	val[50%:]	(Bilen et al., 2017)
ucf101	85.96	87.70	train	val[:50%]	val[50%:]	(Bilen et al., 2017)
aircraft	72.95	70.01	train	val[:50%]	val[50%:]	(Bilen et al., 2017)
dtd	73.11	75.00	train	val[:50%]	val[50%:]	(Bilen et al., 2017)
vgg-flowers	99.37	99.41	train	val[:50%]	val[50%:]	(Bilen et al., 2017)
Multitask Character Classification Benchmark						
emnist/digits	99.86	99.81	train[5%:]	train[:5%]	test	(Cohen et al., 2017)
emnist/letters	96.57	95.03	train[5%:]	train[:5%]	test	(Cohen et al., 2017)
kmnist	99.79	98.44	train[5%:]	train[:5%]	test	(Clanuwat et al., 2018)
mnist	99.83	99.72	train[5%:]	train[:5%]	test	(LeCun et al., 1998)
omniglot	99.89	99.90	train	small1	small2	(Lake et al., 2015)
cmaterdb/bangla	99.89	99.00	train[20%:]	train[:20%]	test	(Das et al., 2012b;a)
cmaterdb/devanagari	100	98.20	train[20%:]	train[:20%]	test	(Das et al., 2012b;a)
cmaterdb/telugu	100	99.40	train[20%:]	train[:20%]	test	(Das et al., 2012b;a)
VTAB 1k benchmark <sup>[4]</sup>						
caltech101	98.97	89.88	train[:800]	train[2754:2954]	test	(Fei-Fei et al., 2004)
cifar100	96.92	92.85	train[:800]	train[45000:45200]	test	(Krizhevsky, 2009)
cifar10	100	99.23	train[:800]	train[45000:45200]	test	(Krizhevsky, 2009)
dtd	82.05	77.87	train[:800]	val[:200]	test	(Cimpoi et al., 2014)
oxford_flowers102	100	99.33	train[:800]	val[:200]	test	(Nilsback & Zisserman, 2008)
oxford_iiit_pet	97.44	93.51	train[:800]	train[2944:3144]	test	(Parkhi et al., 2012)
sun397	66.15	60.93	train[:800]	val[:200]	test	(Xiao et al., 2010)
svhn_cropped	98.00	97.47	train[:800]	train[65931:66131]	test	(Netzer et al., 2011)
patch_camelyon	96.41	91.55	train[:800]	val[:200]	test	(Veeling et al., 2018)
eurosat/rgb	99.49	98.56	train[:800]	train[16200:16400]	train[21600:]	(Helber et al., 2019)
resisc45	97.50	95.33	train[:800]	train[18900:19100]	train[25200:]	(Cheng et al., 2017)
diabetic_retinopathy_detection/...						
btgraham-300	88.50	82.77	train[:800]	val[:200]	test	(Kaggle & EyePacs, 2015)
clevr/count_cylinders <sup>[5]</sup>	99.49	99.01	train[:800]	train[63000:63200]	val	(Johnson et al., 2017)
clevr/count_all	100	99.88	train[:800]	train[63000:63200]	val	(Johnson et al., 2017)
clevr/closest_object_distance	92.00	90.64	train[:800]	train[63000:63200]	val	(Johnson et al., 2017)
dmlab	77.44	74.71	train[:800]	val[:200]	test	(Zhai et al., 2019)
dsprites/label_x_position	100	99.43	train[:800]	train[589824:590024]	train[663552:]	(Klindt et al., 2021)
dsprites/label_orientation	97.50	96.30	train[:800]	train[589824:590024]	train[663552:]	(Klindt et al., 2021)
kitti/closest_object_distance <sup>[5]</sup>	84.50	78.34	train[:800]	val[:200]	test	(Geiger et al., 2012)
kitti/count_vehicles <sup>[5]</sup>	93.85	69.34	train[:800]	val[:200]	test	(Geiger et al., 2012)
kitti/closest_vehicle_distance	88.00	82.14	train[:800]	val[:200]	test	(Geiger et al., 2012)
smallnorb/label_category <sup>[5]</sup>	100	97.67	train[:800]	test[:200]	test[50%:]	(LeCun et al., 2004)
smallnorb/label_lighting <sup>[5]</sup>	100	98.30	train[:800]	test[:200]	test[50%:]	(LeCun et al., 2004)
smallnorb/label_azimuth	37.00	33.75	train[:800]	test[:200]	test[50%:]	(LeCun et al., 2004)
smallnorb/label_elevation	92.50	92.83	train[:800]	test[:200]	test[50%:]	(LeCun et al., 2004)
Continues in Table 6 ...						

Table 6: Datasets details (part 3 of 3).

Name	Accuracy (%)		Splits			Reference
	Val.	Test	Train	Val.	Test	
... Continues from Table 5						
<b>Task-set B</b>						
beans	100	94.53	train	val	test	(Makerere, 2020)
binary_alpha_digits	91.43	85.71	train[10%:]	train[5%:10%]	train[:5%]	–
caltech_birds2010	98.00	89.48	train[5%:]	train[:5%]	test	(Welinder et al., 2010)
caltech_birds2011	93.00	90.94	train[5%:]	train[:5%]	test	(Welinder et al., 2010)
cars196	89.23	87.18	train[5%:]	train[:5%]	test	(Krause et al., 2013)
cassava	92.31	91.78	train	val	test	(Mwebaze et al., 2019)
cats_vs_dogs	100	99.83	train[10%:]	train[5%:10%]	train[:5%]	(Elson et al., 2007)
citrus_leaves	100	93.33	train[10%:]	train[5%:10%]	train[:5%]	(Rauf et al., 2019)
colorectal_histology	99.17	98.40	train[10%:]	train[5%:10%]	train[:5%]	(Kather et al., 2016)
controlled_noisy_web_labels/...						
mini_imagenet_red	96.35	95.04	train_00	val[:50%]	val[50%:]	(Jiang et al., 2020)
mini_imagenet_blue	96.35	95.24	train_00	val[:50%]	val[50%:]	(Jiang et al., 2020)
curated_breast_imaging_ddsm/...						
patches	70.66	67.49	train	val	test	(Clark et al., 2013)
cycle_gan/...						
apple2orange	100	98.83	trainA+B[10%:]	trainA+B[:10%]	testA+B	(Zhu et al., 2017)
summer2winter	95.71	90.49	trainA+B[10%:]	trainA+B[:10%]	testA+B	(Zhu et al., 2017)
horse2zebra	100	99.23	trainA+B[10%:]	trainA+B[:10%]	testA+B	(Zhu et al., 2017)
monet2photo	100	100	trainA+B[10%:]	trainA+B[:10%]	testA+B	(Zhu et al., 2017)
cezanne2photo	100	100	trainA+B[10%:]	trainA+B[:10%]	testA+B	(Zhu et al., 2017)
ukiyo2photo	100	99.70	trainA+B[10%:]	trainA+B[:10%]	testA+B	(Zhu et al., 2017)
vangogh2photo	100	100	trainA+B[10%:]	trainA+B[:10%]	testA+B	(Zhu et al., 2017)
maps	100	100	trainA+B[10%:]	trainA+B[:10%]	testA+B	(Zhu et al., 2017)
cityscapes	100	100	trainA+B[10%:]	trainA+B[:10%]	testA+B	(Zhu et al., 2017)
facades	100	100	trainA+B[10%:]	trainA+B[:10%]	testA+B	(Zhu et al., 2017)
iphone2dslr_flower	98.99	94.66	trainA+B[10%:]	trainA+B[:10%]	testA+B	(Zhu et al., 2017)
deep_weeds	98.79	98.06	train[10%:]	train[5%:10%]	train[:5%]	(Olsen et al., 2019)
domainnet/real	90.90	90.25	train[5%:]	train[:5%]	test	(Peng et al., 2019)
domainnet/painting	82.62	82.11	train[5%:]	train[:5%]	test	(Peng et al., 2019)
domainnet/clipart	87.16	85.35	train[5%:]	train[:5%]	test	(Peng et al., 2019)
domainnet/quickdraw	74.34	73.78	train[5%:]	train[:5%]	test	(Peng et al., 2019)
domainnet/infograph	56.28	55.28	train[5%:]	train[:5%]	test	(Peng et al., 2019)
domainnet/sketch	78.70	78.51	train[5%:]	train[:5%]	test	(Peng et al., 2019)
food101	94.58	91.47	train[5%:]	val	train[:5%]	(Bossard et al., 2014)
horses_or_humans	100	99.61	train[5%:]	train[:5%]	test	(Moroney, 2019a)
i_naturalist2017	77.27	77.71	train	val[:50%]	val[50%:]	(Horn et al., 2018)
i_naturalist2018	80.90	80.97	train	val[:50%]	val[50%:]	(Horn et al., 2018)
imagenet_a	87.78	84.53	train[10%:]	train[5%:10%]	train[:5%]	(Hendrycks et al., 2021b)
imagenet_lt	87.26	82.50	train	val	test	(Liu et al., 2019c)
imagenet_r	91.13	89.87	train[10%:]	train[5%:10%]	train[:5%]	(Hendrycks et al., 2021a)
imagenet_sketch	89.54	88.60	train[10%:]	train[5%:10%]	train[:5%]	(Wang et al., 2019a)
imagenette	99.92	100	train[5%:]	val	train[:5%]	(Howard, 2019a)
imagewang	97.32	99.59	train[5%:]	val	train[:5%]	(Howard, 2019b)
malaria	98.17	97.46	train[10%:]	train[5%:10%]	train[:5%]	(Rajaraman et al., 2018)
pet_finder	62.40	60.73	train[10%:]	train[5%:10%]	train[:5%]	–
places365_small	58.99	59.15	train	val[:50%]	val[50%:]	(Zhou et al., 2018)
plant_village	100	99.89	train[10%:]	train[5%:10%]	train[:5%]	(Hughes & Salathé, 2015)
plantae_k	99.05	90.74	train[10%:]	train[5%:10%]	train[:5%]	(Kour & Arora, 2019)
quickdraw_bitmap	78.35	77.59	train[20k:]	train[10k:20k]	train[:10k]	(Ha & Eck, 2018)
rock_paper_scissors	100	97.04	train[5%:]	train[:5%]	test	(Moroney, 2019b)
siscore/rotation	100	100	train[10%:]	train[5%:10%]	train[:5%]	(Djulonga et al., 2021)
siscore/size	99.93	99.94	train[10%:]	train[5%:10%]	train[:5%]	(Djulonga et al., 2021)
siscore/location	99.99	99.95	train[10%:]	train[5%:10%]	train[:5%]	(Djulonga et al., 2021)
stanford_dogs	95.17	93.50	train[5%:]	train[:5%]	test	(Khosla et al., 2012)
stanford_online_products	90.00	89.47	train	test[:10k]	test[10k:]	(Song et al., 2016)
stl10	100	99.64	train[5%:]	train[:5%]	test	(Coates et al., 2011)
tf_flowers	99.45	97.83	train[10%:]	train[5%:10%]	train[:5%]	–
uc_merced	100	100	train[10%:]	train[5%:10%]	train[:5%]	(Yang & Newsam, 2010)

---

**Algorithm 1** Pseudocode for one active task iteration

---

```
1: Active task:  $t$ 
2: Set of all the models currently in the multitask system:  $\mathcal{M}$ 
3: Active population:  $\mathcal{A} \leftarrow \{m \mid m \in \mathcal{M} \wedge m \text{ trained on } t\}$ 
4: for  $\#generations$  do
5:   for  $\#child-models$  do
6:     ▷ Sample parent model
7:     Parent model:  $p \leftarrow \mathbf{none}$ 
8:     for Candidate parent model:  $\hat{p} \in [sorted_{score}(\mathcal{A}), sorted_{random}(\mathcal{M} \setminus \mathcal{A})]$  do
9:       if  $0.5^{\#selections(\hat{p}, t)} > x \sim Uniform([0, 1])$  then
10:         $p \leftarrow \hat{p}$ 
11:        break
12:       end if
13:     end for
14:     if  $p = \mathbf{none}$  then
15:        $p \sim Uniform(\mathcal{A} \cup \mathcal{M})$ 
16:     end if
17:     ▷ Sample child model
18:     Set of mutations:  $\Delta \leftarrow \{make-trainable-head\}$ 
19:     for Candidate mutation:  $\hat{\delta} \in possible-mutations(p)$  do
20:       if  $\mu(\hat{\delta}|p) > x \sim Uniform([0, 1])$  then
21:          $\Delta \leftarrow \Delta \cup \{\hat{\delta}\}$ 
22:       end if
23:     end for
24:     Untrained child model:  $c_0 \leftarrow apply-mutations(p, \Delta)$ 
25:     ▷ Train child model
26:     Retained child model:  $c \leftarrow \mathbf{none}$ 
27:     for  $i \in [1, \dots, \#train-cycles]$  do
28:        $c_i \leftarrow train(c_{i-1}, \min(1 \text{ epoch}, \#samples-cap))$ 
29:       if  $score(c_i) \geq \max(\{score(c) \mid c \neq \mathbf{none}\} \cup \{score(p) \mid p \text{ trained on } t\} \cup \{-\infty\})$  then
30:          $c \leftarrow c_i$ 
31:       end if
32:     end for
33:     if  $c \neq \mathbf{none}$  then
34:        $\mathcal{A} \leftarrow \mathcal{A} \cup \{c\}$ 
35:     end if
36:   end for
37: end for
38:   ▷ Keep only the best model for  $t$ 
39:  $\mathcal{M} \leftarrow \{\operatorname{argmax}_{m \in \mathcal{A}} score(m)\} \cup \{m \mid m \in \mathcal{M} \wedge m \text{ not trained on } t\}$ 
```

---